GA–A27954

COMPATIBILITY OF INTERNAL TRANSPORT BARRIER WITH STEADY-STATE OPERATION IN THE HIGH BOOTSTRAP FRACTION REGIME ON DIII-D

by

A.M. GAROFALO, X. GONG, Q. REN, W.M. SOLOMON, E.J. STRAIT, M.A. VAN ZEELAND, C.T. HOLCOMB, B. WAN, R. BRAVENEC, R.V. BUDNY, S. DING, B.A. GRIERSON, L.L. LAO, G. LI, J. QIAN,*G.M. STAEBLER, and G. XU

SEPTEMBER 2014

GENERAL ATOMICS

DISCLAIMER

GA–A27954

COMPATIBILITY OF INTERNAL TRANSPORT BARRIER WITH STEADY-STATE OPERATION IN THE HIGH BOOTSTRAP FRACTION REGIME ON DIII-D

by

A.M. GAROFALO, X. GONG,* Q. REN,* W.M. SOLOMON,† E.J. STRAIT, M.A. VAN ZEELAND, C.T. HOLCOMB,‡ B. WAN,* R. BRAVENEC,¶ R.V. BUDNY,† S. DING,* B.A. GRIERSON,† L.L. LAO, G. LI,* J. QIAN,* G.M. STAEBLER, and G. XU*

This is a preprint of a paper to be presented at the Twenty-Fifth IAEA Fusion Energy Conf., October 13-18, 2014 in Saint Petersburg, Russia, and published in the *Proceedings*.

*Institute of Plasma Physics Chinese Academy of Sciences, Hefei, China.
†Princeton Plasma Physics Laboratory, Princeton, New Jersey.
‡Lawrence Livermore National Laboratory, Livermore, California.
¶Fourth State Research, 503 Lockhart Dr., Austin, TX 78704.

Work supported in part by
the U.S. Department of Energy
under DE-FC02-04ER54698, DE-AC02-09CH11466
and DE-AC52-07NA27344

GENERAL ATOMICS PROJECT 30200
SEPTEMBER 2014

GENERAL ATOMICS

Compatibility of Internal Transport Barrier with Steady-State Operation in the High Bootstrap Fraction Regime on DIII-D

PPC/P2-31

A.M. Garofalo[1], X. Gong[2], Q. Ren[2], W.M. Solomon[3], E.J. Strait[1], M.A. Van Zeeland[1], C.T. Holcomb[4], B. Wan[2], R. Bravenec[5], R.V. Budny[3], S. Ding[2], B.A. Grierson[3], J.M. Hanson[6], W.W. Heidbrink[7], L.L. Lao[1], G. Li[2], C.C. Petty[1], J. Qian[2], G.M. Staebler[1], and G. Xu[2]

[1]General Atomics, PO Box 85608, San Diego, CA 92186-5608, USA.
[2]Institute of Plasma Physics Chinese Academy of Sciences, 350 Shushanhu Rd, Hefei, Anhui 230031, China.
[3]Princeton Plasma Physics Laboratory, PO Box 451, Princeton, NJ 08543-0451, USA
[4]Lawrence Livermore National Laboratory, 7000 East Ave, Livermore, CA 94550, USA
[5]Fourth State Research, 503 Lockhart Dr., Austin, TX 78704, USA
[6]Columbia University, 116th St and Broadway, New York, NY 10027-6900, USA
[7]University of California Irvine, University Dr., Irvine, CA92697, USA
email address for first author: garofalo@fusion.gat.com

Abstract. Recent DIII-D research has increased confidence in the applicability of the high bootstrap current fraction plasma regime for the realization of a steady-state fusion reactor. Fully noninductive plasmas have been sustained for long durations with large-radius ITBs, bootstrap fraction≥80%, $\beta_N \leq 4$, $\beta_P \geq 4$, and $\beta_T \geq 2\%$. Building on earlier DIII-D work [P.A Politzer, et al., Nucl. Fusion **45**, 417 (2005)], the new experiments utilized an approach to fully noninductive operation based on removing the current drive by transformer induction. The plasmas exhibit excellent energy confinement quality, with $H_{98y2} \sim 1.5$. The excellent confinement is associated with the formation of an ITB at large minor radius in all channels (n_e, T_e, T_i, rotation). The ITB is maintained at large minor radius for ~4 s, more than three times the current profile relaxation time, τ_{CR} estimated to be ~1 s. The ITB is maintained at large minor radius despite edge localized mode perturbations, which become particularly large as β_N is pushed against the global ideal-wall limit. The transient stored energy drops caused by these coupled edge-core modes have been previously referred to as "relaxation oscillations". The maximum achievable β_N is limited by the stability of these modes, and depends on the plasma-wall separation, which is in turn dictated by the operational need to reduce wall heating by fast ion losses. Using an optimized outer gap waveform has enabled a ~30% β_N increase relative to earlier work, and opened the path to further optimizations and performance improvements.

1. Introduction

A high bootstrap current fraction plasma regime is desirable for steady-state tokamak operation because it reduces the demands on external noninductive current drive. Often, this regime is characterized by high β_N and an internal transport barrier (ITB), leading to concerns about stability limits and profile control with reduced external input (power). Recent DIII-D research has increased confidence in the potential of the high bootstrap fraction approach for applicability to a steady state fusion reactor. This effort was largely motivated by the interest in the developing and testing a possible scenario for steady-state advanced tokamak demonstration on EAST [1]. Building on earlier JT-60U and DIII-D work [2,3], a joint team of DIII-D and EAST teams adopted an approach to fully noninductive operation based on high β_P ($\beta_P \geq 3$) operation without the current drive by transformer induction. Utilizing new DIII-D capabilities and diagnostics with improved time and spatial resolutions, these experiments have led to increased physics understanding of the performance limitations, and ultimately to increased plasma performance.

Experiments on JT-60U had shown that sustainment of large ITB radius was attained only in high β_P discharges, with larger radius obtained with larger f_{BS}. High confinement could be sustained in negative central magnetic shear (NCS) plasmas as long as a large $\varrho(q_{min})$ could be sustained by noninductive (bootstrap or external) current drive. Although low I_p (0.8 MA)

high q operation ($q_{95}\approx 9$) was necessary to sustain large $\varrho(q_{min})$ with the current drive capabilities of JT-60U, that research suggested that steady-state high confinement NCS plasmas could be obtained in a lower q and higher β_T regime with more off-axis current drive power. The maximum β_N achieved in the JT-60U experiments was limited to about 2, probably because of lack of wall-stabilization of the n=1 kink mode at the time of that research. Access to the wall-stabilized regime on JT-60U was only possible after 2005, when ferritic steel tiles were installed to reduce the magnetic field ripple and enable operation with reduced plasma-wall outer gap.

Taking advantage of wall-stabilization [4], high β_P experiments on DIII-D had achieved $\beta_N \approx \beta_P \sim 3$, and $\beta_T \sim 1.5\%$. To address reactor relevant issues of control near the beta limit in fully noninductive conditions with very high bootstrap fraction, those experiments fixed the current in the transformer coil after the current flattop was reached. The achievable plasma current and pressure were limited by a relaxation oscillation, described as the repetitive buildup and collapse of an ITB at large minor radius. These relaxation oscillations had been attributed to a misalignment between the bootstrap and the externally driven non-inductive current densities [5].

In the recent DIII-D experiments, fully noninductive plasmas have been sustained for long durations with bootstrap fraction $f_{BS} \geq 80\%$ and large-radius ITBs. Relaxation oscillations have been observed to limit the plasma performance in these experiments as well, but the main cause is identified as the n=1 ideal-wall external kink mode, primarily affecting the H-mode pedestal and in some cases also the ITB. This hypothesis was tested by performing a scan of the outboard plasma-wall gap, which resulted in the extension of the plasma performance to $\beta_N \approx \beta_P \sim 4$, and $\beta_T \sim 2\%$. The implications of this result are that ITBs can be compatible with steady-state operation at beta within the n=1 ideal-wall limit.

2. Fully Noninductive Operation

Figure 1 shows time histories of several plasma parameters for a representative fully noninductive, high β_P discharge with performance similar to the previous DIII-D results. The plasma cross section is an upper biased double-null divertor shape, with elongation $\kappa \sim 1.86$ and average triangularity (top and bottom) ~0.6. The toroidal field is $B_T = 2$ T. After an approximate equilibrium is established (1.7 s) the current in the transformer coil is fixed, so that the plasma current is forced to relax noninductively. A flattop at approximately 0.6 MA is maintained by increasing β_N and thus the bootstrap current fraction, until a 100% noninductive condition, as shown by the ~zero loop voltage signal, is achieved and maintained for the rest of the discharge duration, limited by hardware constraints on DIII-D pulse length. This discharge achieves and maintains $\beta_N \sim \beta_P \geq 3$ and $\beta_T \sim 1.5\%$ using a total heating and current power of ~11 MW. This power includes ~5 MW of off-axis neutral beam injection (NBI) ($\rho \sim 0.4$), and 2.5 MW of off axis electron cyclotron current drive (ECCD), injected at $\rho \sim 0.5$.

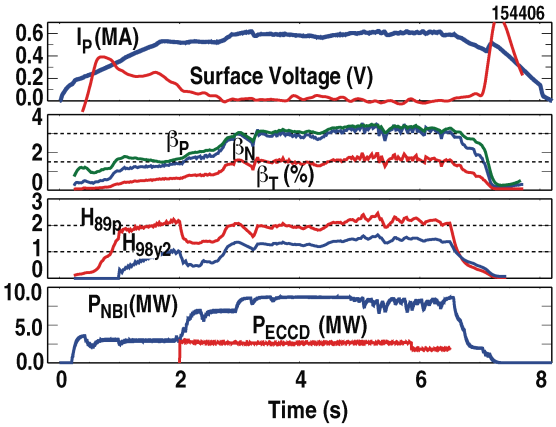

Fig. 1. Time traces of selected plasma parameters for representative high β_P discharge 154406.

This plasma exhibits excellent energy confinement quality, with confinement enhancement factor over H-mode confinement scaling H_{98y2} up to ~1.5. The exceeding of $H_{98y2} \sim 1$ is associated with the formation of an ITB at large minor radius ($\rho \sim 0.7$) in all channels (n_e, T_e, T_i, rotation), shown in Fig. 2. The ion heat diffusivity calculated by TRANSP [6] is shown to drop to the neoclassical predicted levels, $\chi_{i,CH}$ [7], at $\rho \sim 0.7$, indicating strong reduction of transport and confirming the presence of an ITB. It is

surprising that the ion heat diffusivity is actually lower than the neoclassical prediction throughout the core ($\rho < 0.7$). Simulations of non-local effects with GTC-NEO [8] give core neoclassical diffusivity below $\chi_{i,CH}$. Non-local effects may be due to the low plasma current.

Note that the q-profile does not necessarily show an absolute minimum near the location of the ITB. In many cases, similar to discharge 154406, the q-profile is near monotonic, with a local minimum at $\rho \sim 0.6$, similar to what was reported previously [3]. However, no adverse or beneficial effect has been observed in cases where, due to stronger early heating, the q-profile develops strong shear reversal in the core, with very high central safety factor $q_0 \sim 10$ maintained throughout the discharge. Also, sustainment of the ITB at a large radius is not tied to the use of off-axis external current drive. Sustained high q_{min} and large radius ITB are observed with or without off-axis NBI [9], and with or without off-axis ECCD, as was reported in Ref. [3].

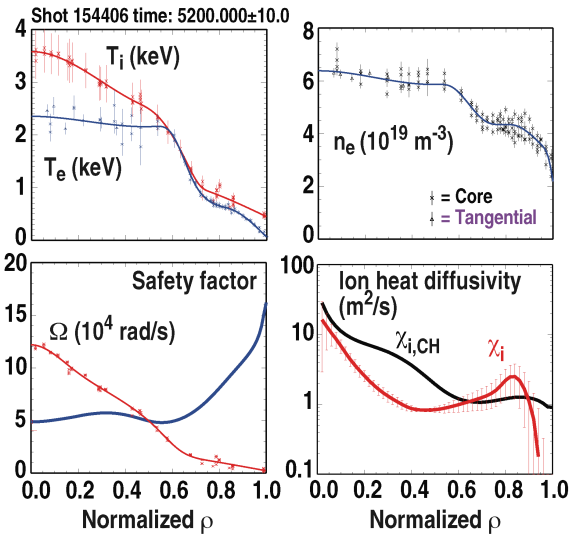

Fig. 2. Radial profiles for discharge 154406 at t = 5.2 s, showing ITB at $\rho \sim 0.7$.

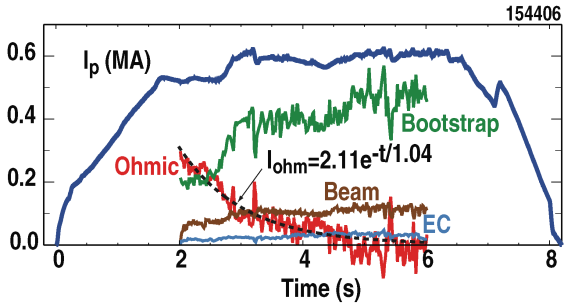

Fig. 3. Time traces of total plasma current I_p (blue) and its components: bootstrap (green), beam driven (brown), EC driven (azul), and Ohmic (red). Dashed black line is the exponential fit of the Ohmic component. Spikes in the traces are due to the relaxation oscillations, discussed in Sec. 4. Discharge 154406.

The various current components for discharge 154406, plotted in Fig. 3, are calculated from experimental profiles by the TRANSP code. The bootstrap current fraction reaches up to 80%–85%, the NBI-driven current fraction is 15%–20%, and only <5% of the total current is driven by EC frequency electromagnetic waves, since the efficiency of ECCD is low at large minor radius. Note that despite having the transformer coil current clamped, some loop voltage may be driven by current variations in the shaping and vertical field coils. An exponential fit to the calculated Ohmic current yields a time constant of ~1.06 s. This is in close agreement with the current profile relaxation time estimated as τ_{CR} = 0.17*R/Resistance = 1–1.2 s [10] between 2 and 6 s in this discharge, therefore supporting that the plasma current is indeed relaxing noninductively.

3. MHD Stability Limits and Fast Ion Losses

Stability analysis shows that these high β_P discharges operate against the MHD stability limit with an ideal wall at the position of the DIII-D wall. As an example, this section discusses equilibrium and stability analysis for discharge 154366, which maintains high $\beta_N \geq 3$ with small, infrequent relaxation oscillations (discussed in Sec. 4). Figure 4 shows two kinetic equilibrium reconstructions for t = 4.185 s, shortly before a relaxation oscillation event. The cross section of plasma and conducting vessel shows the large plasma-wall gap at the outer midplane, of about ~14 cm. This should be compared with more routine DIII-D operation using an outer gap of 8–10 cm. In addition to the extensive set of measurements available for equilibrium reconstruction at DIII-D, these reconstructions use a bootstrap current model to further constrain the edge current density at minor radius $0.8 < \rho < 1$, a reasonable approach since the analysis time is more than two current profile relaxation times after the clamping of

the transformer coil. The edge bootstrap current densities predicted by the Sauter model [11] and the first principle kinetic code Neo [12] are used as constraints (respectively solid and dashed lines in Fig. 4). For this discharge, the two models differ only slightly (about 10%), with the Neo bootstrap model yielding a slightly better fit of the experimental measurements. However, in cases with higher pedestal density, leading to higher collisionality, it was found [13] that the Sauter formula significantly over-predicts the bootstrap current, a finding that supports recent theoretical work by Belli [14].

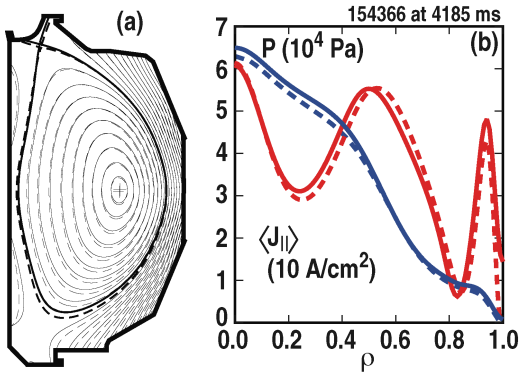

Fig. 4. Equilibrium reconstructions for discharge 154366 at t = 4.185 s. Solid (dashed) curves show results using the Sauter (Neo) model as edge current constraint. (a) Cross section of plasma and limiter wall; (b) Radial profiles of the plasma pressure and flux averaged parallel current density.

Ideal MHD calculations of the *n*=1 kink mode stability with an ideal wall approximating closely the shape of the DIII-D vessel are shown in Fig. 5 for the two reconstructions, using Sauter and Neo bootstrap current. The stability code allows us to vary the minor radius of the ideal wall, to test the effect of plasma-wall separation on the instability. The plasma is calculated to be at marginal stability with the ideal wall at the position of the DIII-D wall. The mode structure shows large internal components driven by the pres-sure gradients at the ITB. Nevertheless, this is an external mode that can be stabilized by a sufficiently close conducting wall.

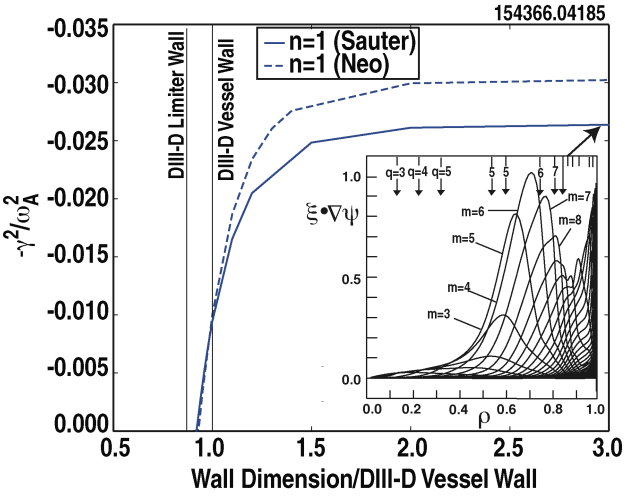

Fig. 5. Calculated growth rate of the *n*=1 ideal kink mode normalized to the Alfvén frequency vs ideal wall dimension multiplier relative to the DIII-D vessel wall for discharge 154366 at t = 4.185 s. Solid (dashed) curve shows results for an equilibrium reconstruction using the Sauter (Neo) model as edge current constraint. Inset shows the mode structure for the ideal wall far away from the plasma.

Indeed, these experiments used a large plasma-wall gap to reduce wall heating by fast ion losses. At relatively low plasma current and large NBI power, the compound losses from classical (due to large orbits) and anomalous [due to Alfvén eigenmodes (AEs) and possibly other instabilities] effects can be significant and can lead to overheating and damage of the limiter tiles. However, recent detailed analysis [15] has shown that the anomalous fast ion losses are high mostly during the β_N and density ramp-up phase, i.e. when the NBI power has increased significantly but the density has not yet reached flattop. This understanding has opened the possibility of developing an optimized waveform of the outer gap that could increase the ideal-wall limit without leading to unacceptable levels of wall over-heating. A summary of the fast ion loss analysis is shown in Fig. 6. The measured neutron rate and stored energy for discharge 154406 are compared to TRANSP calculations using three different levels of beam ion diffusivity (DB=0, 0.5, and 5.0 m^2/s) as well as a temporally varying diffusivity. The variable diffusivity coefficient was derived by interpolating the results of the constant diffusivity runs. In all cases the beam ion diffusivity is constant in radius. Panel 6(d) shows that the required diffusivity changes significantly over time, and roughly tracks the AE mode activity visible in the spectra calculated from the CO_2 interferometer [Fig. 6(a)]. The time-varying

anomalous fast ion losses may be understood as the result of the interplay between the AE activity and the plasma density. As the density increases, the fast ion slowing down time decreases, accomplishing two tasks: the AE instability drive is reduced, and the fast ions displaced by the AE instabilities travel shorter distances prior to thermalization. Both effects lead to reduced fast ion losses. The pedestal density is particularly effective at slowing down the fast ions because of the longer paths travelled at larger minor radius. Once the density has reached a sufficiently high flattop, the inferred fast ion losses are reduced to near classical levels, despite the very high values of q_{min} which can be associated with stronger AE drive through coupling to higher order resonances.

4. Relaxation Oscillations: Edge Localized Modes (ELMs) and ITB

Similar to the earlier DIII-D experiments in the high β_P regime [3], relaxation oscillations have been observed to limit the plasma performance in these new experiments as well. However, thanks to high time resolution measurements, here the oscillations are identified as the repetitive buildup and collapse of the H-mode pedestal, not the ITB. Usually, the ITB persists through the oscillations in stored energy, while the H-mode pedestal is significantly reduced. This section presents an example of this observations, together with evidence that the main cause of the relaxation oscillations is the coupling of ELMs with the marginally stable, ideal-wall n=1 external kink mode. The implication of this hypothesis is that the relaxation oscillations could be ameliorated and the plasma performance improved by increasing the ideal-wall beta limit, for example by reducing the plasma-wall separation gap. This suggestion was tested in the experiments, and the successful results are also shown in this section.

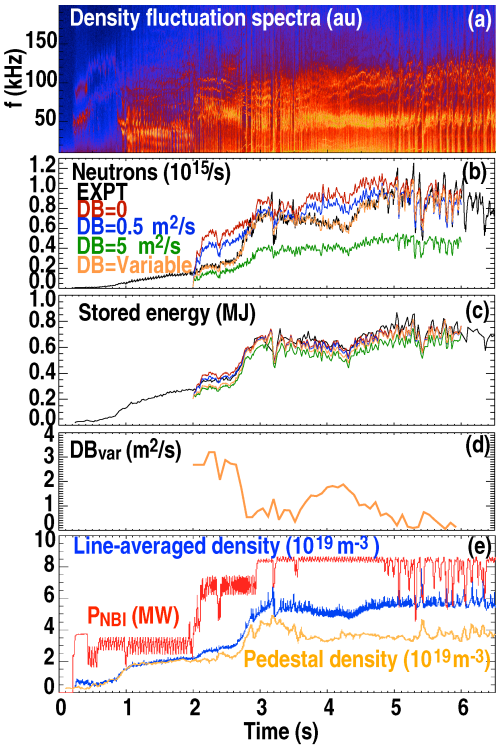

Fig. 6. Time evolution of (a) combined frequency spectra of line-integrated density fluctuations from four CO_2 interferometer chords, (c) the measured and calculated stored energy (calculations are carried out using different values of the spatially-uniform beam-ion diffusion coefficient DB). (d) Time varying value of DB required to match the neutron rate. (e) Time evolution of the line averaged electron density, pedestal density, and NBI power.

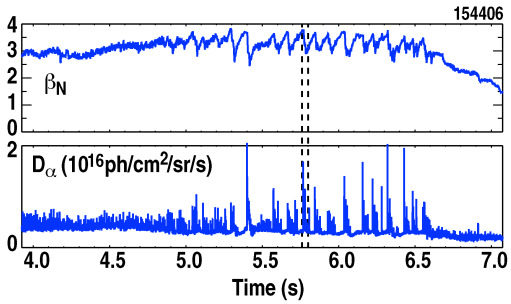

Fig. 7. Time traces of β_N and D_α light, showing large ELMs and the relaxation oscillation effect on the stored energy. Vertical dashed lines show the time range expanded in Fig. 8.

Figure 7 shows the strong impact of the oscillations on the β_N waveform. Once β_N is pushed above 3, the ELMs become particularly large. Larger ELMs cause deeper and broader excursions in the stored energy, which often trip off one or more neutral beams by the sudden increase in base pressure near the beam ducts. In some cases, a large ELM is followed by a total collapse of the stored energy, and in a few cases even by a current disruption.

Figure 8 takes a detailed look into one of these stored energy oscillations, in the time range between vertical dashed lines in Fig. 7. The stored energy drop is caused by a rapid series of short bursts of an n=1 mode. The time scales for growth/decay is ~100 μs, and the

rotation is ~1 kHz. The time evolution of the electron temperature profile, Fig. 8(a,e) shows that the consequence of these bursts is a large reduction of the edge temperature and a much smaller reduction of the core temperature, i.e. an abatement of the large H-mode pedestal and a slight inward movement of the ITB. The bursty n=1 events appear to be relaxation instabilities driven by pedestal gradients and dominated by n=1, rather than higher n as most ELMs are. The rapid decay could be a result of the mode reducing the driving gradient. The first n=1 burst usually has a shorter growth time (<100 μs), more localized spatial structure, and larger spike signature in the photo-diode D_α signal, all characteristics of an ELM. The following bursts have longer growth time (≥200 μs) and more sinusoidal n=1 spatial structure. This slower growth compared to a standard ELM is consistent with an n=1 kink mode occurring at the ideal MHD stability limit, and is discussed later in this section.

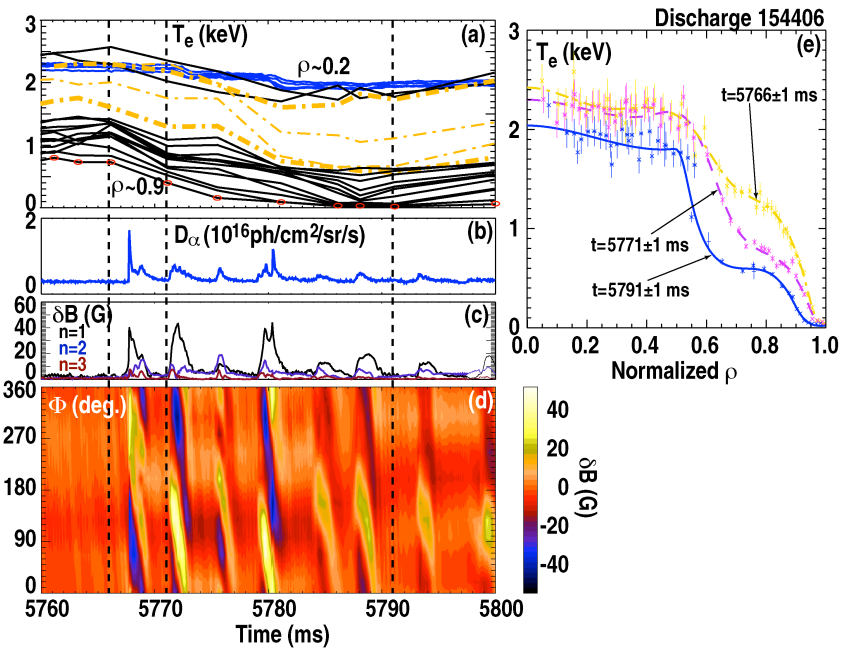

Fig. 8. Time evolution of (a) electron temperature measured by Thomson scattering at 0.2 ≤ ρ ≤ 0.9, and by ECE at 0.2 ≤ ρ ≤ 0.3; (b) D_α light; (c) n=1,2, and 3 components of the perturbed magnetic field at the outer midplane measured by poloidal field sensors. (d) Color coded contour plot of the perturbed poloidal field vs time and toroidal angle. (e) Radial pro-files of the electron temperature at times indicated by vertical dashed lines.

Figure 9 shows the results of an experimental test of the ideal-wall limit effect, using a scan of the plasma-wall outer gap. The input for the two discharges shown differs only in the programmed waveform for the plasma-wall outer gap. Discharge 159206 with the larger gap (the previous standard for this low current regime) suffers a beta collapse and disruption at $\beta_N \sim 3.6$. Discharge 159213 exceeds this β_N value, and sustains $\beta_N \leq 4$ until the high NBI power phase ends. This macroscopic demonstration of the wall stabilization effect provides support for the accuracy of the ideal MHD calculations of the ideal-wall stability limit presented in the previous section.

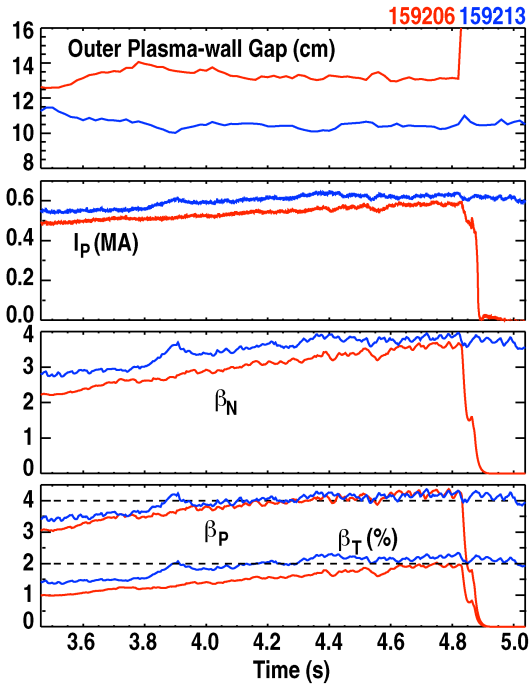

Fig. 9. Time traces of selected plasma parameters for similar discharges with only input difference in the plasma-wall outer gap.

In discharge 159206, β_N reaches a value of about 3.6, or about 5 times the internal inductance l_i, at which point (t ~ 4830 ms) the plasma disrupts due to a rapidly growing instability. The instability is consistent with an n=1 kink mode occurring at the ideal MHD

stability limit. Just before the instability, data from the toroidal array of Mirnov loops show a large, single filament-like pulse that grows and decays in about 200 μs, while making almost two toroidal rotations. This is a typical magnetic signature of an ELM. The large ELM leads directly into the n=1 mode growing to large amplitude (~60 G) with a rotation frequency $\omega/2\pi \sim 1$ kHz and a growth time of $\tau_g \sim 250$ μs (Fig. 10).

While the large n=1 mode is the ultimate disruption cause, the immediately preceding ELM is a particularly large one, probably because its low n components are amplified by proximity to the global ideal-wall stability limit. The measured growth time of the n=1 mode is consistent with an ideal mode slowly driven through the stability boundary: $\tau_g = \tau_{MHD}^{2/3} \tau_h^{1/3}$ [16], where τ_{MHD} is of the order of the expected growth time of the ideal MHD mode and τ_h is the time scale for the increase of the instability drive. For a global kink-ballooning mode, the instability drive is provided by both high plasma pressure (high β_N) and high current density near the plasma edge (low l_i). Therefore the instability drive in this case is proportional to the ratio β_N/l_i. Here, l_i is nearly constant while β_N is ramping up with a rise time $\tau_h \sim 3$ s, and the measured growth time of the kink mode is $\tau_g = 250$ μs, which yield $\tau_{MHD} \sim 2$ μs. This time is indeed consistent with expectations for ideal MHD instabilities. Therefore, the experimentally observed growth time of ~250 μs is consistent with an ideal kink mode slowly driven through the ideal-wall limit.

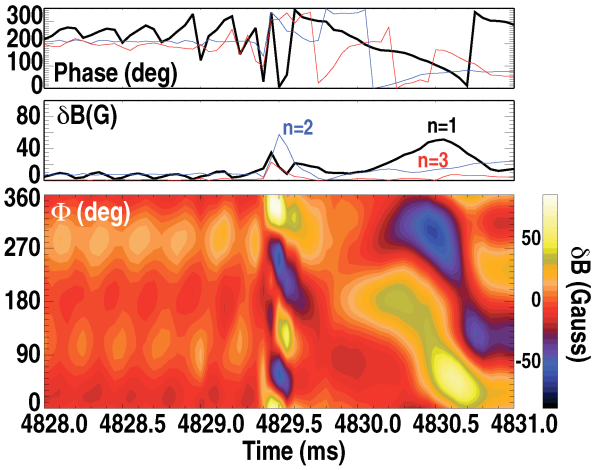

Fig. 10. Analysis of perturbed poloidal field measurements in discharge 159206 at times just before the disruption.

Further optimization of the scenario waveforms has led to additional improvements in the achievable plasma performance, with maximum β_N up to 4.3, β_P up to 4.5, β_T up to 3%, and ratio β_N/l_i up to >8. The scatter plots in Fig. 11 are from a database comprising the last 20 discharges of these experiments. A clear trend is observed, with both wall stabilization, measured by the ratio β_N/l_i, and absolute performance, measured by either β_N, or β_P, or β_T, strongly improving with reducing the outer gap. The maximum values of β_N/l_i and of β_P are among the highest ever observed on DIII-D. It is particularly remarkable that these record values are achieved in plasmas with ITBs. These results are a clear demonstration that ITB plasmas are compatible with high beta limits, as long as the ITB is at large minor radius and the conducting wall is sufficiently close to the plasma, yielding a strong coupling between the kink mode and the wall.

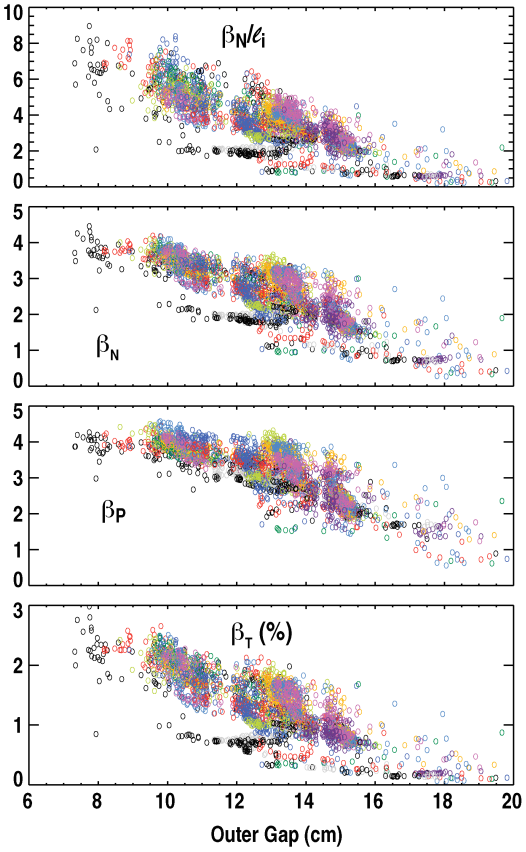

Fig. 11. Scatter plots of β_N/l_i, β_N, β_P, and β_T versus the plasma wall separation at the outboard mid-plane, for a database comprising the last 20 discharges of high β_P experiments analyzed between t = 2 s and t = 6 s.

5. Summary and Conclusions

Recent DIII-D experiments have increased confidence in the potential of the high bootstrap fraction approach for applicability to a steady state fusion reactor. These experiments were largely motivated by the interest in the developing and testing a possible scenario for steady-state advanced tokamak demonstration on EAST. Fully noninductive plasmas have been sustained for long durations with bootstrap fraction $f_{BS} \geq 80\%$, $\beta_N \leq 4$, $\beta_P \geq 4$, and $\beta_T \geq 2\%$, and with excellent energy confinement quality, with $H_{98y2} \sim 1.5$. The excellent confinement is associated with the formation of an ITB at large minor radius in all channels (n_e, T_e, T_i, rotation). An important result, providing evidence of dynamical stability, is that the ITB is maintained at large minor radius despite ELM perturbations, which become particularly large as β_N is pushed against the global ideal-wall limit. The transient stored energy drops caused by these coupled edge-core modes have been previously referred to as "relaxation oscillations". The maximum achievable β_N is limited by the stability of these modes, and depends on the plasma-wall separation, which is in turn dictated by the operational need to reduce wall heating by fast ion losses. During the course of these experiments, it was found that the anomalous fast ion losses are high only during the β_N and density ramp-up phase, i.e. when the NBI power has increased significantly but the density has not yet reached flattop. This understanding led to the development of an optimized waveform of the outer gap to reduce the plasma-wall separation thus increasing the ideal-wall limit without leading to unacceptable levels of wall over-heating. Using this optimized outer gap waveform has enabled a significant (~30%) performance increase relative to earlier work, demonstrating that ITB plasmas can be compatible with high beta limits, and has opened the path to future performance improvements.

This material is based upon work supported in part by the U.S. Department of Energy, Office of Science, Office of Fusion Energy Sciences, using the DIII-D National Fusion Facility, a DOE Office of Science user facility, under Awards DE-FC02-04ER54698, DE-AC02-09CH11466, and DE-AC52-07NA27344.

References

[1] B. Wan, *et al.*, *Proc. of 41st EPS Conf. on Plasma Physics, Berlin* (European Physical Society, 2014) Vol. 38F, paper O2.104.
[2] T. Fujita, *et al.,* Nucl. Fusion **42**, 180 (2002)
[3] P.A. Politzer, *et al.*, Nucl. Fusion **45**, 417 (2005)
[4] A.M. Garofalo, *et al.*, Phys. Rev. Lett. **89**, 235001 (2002)
[5] J.P.S. Bizarro, *et al.*, Nucl. Fusion **47**, L41 (2007)
[6] R.J. Hawryluk, "An Empirical Approach to Tokamak Transport," *Physics of Plasmas Close to Thermonuclear Conditions*, Ed. by B. Coppi, *et al.*, (CEC, Brussels, 1980) Vol. 1, 19
[7] C.S. Chang and F.L. Hinton, Phys. Fluids **25**, 1493 (1982)
[8] W.X. Wang, *et al.*, Computer Phys. Commun. **164**, 178 (2004)
[9] X. Gong, *et al.*, this conference
[10] D.R. Mikkelsen, Phys. Fluids B **1**, 333 (1989)
[11] O. Sauter, *et al.*, Phys. Plasmas **9**, 5140 (2002)
[12] E.A. Belli, *et al.,* Plasma Phys. Control. Fusion **54**, 015015 (2012)
[13] Q. Ren, *et al.,* "Test of Bootstrap Current Models Using High β_p EAST-Demonstration Plasmas on DIII-D," submitted to Plasma Phys. Control. Fusion (2014)
[14] E.A. Belli, *et al.*, Plasma Phys. Control. Fusion **56**, 045006 (2014)
[15] W.W. Heidbrink, *et al.,* Plasma Phys. Control. Fusion **56**, 095030 (2014)
[16] J.D. Callen, *et al.*, Phys. Plasmas **6**, 2963 (1999)